

ICRH-related impurity source and control across experiments in H, D, T plasmas at JET-ILW

Original

ICRH-related impurity source and control across experiments in H, D, T plasmas at JET-ILW / Chomiczewska, A.; Gromelski, W.; Ivanova-Stanik, I.; Kowalska-Strzciwilk, E.; Wendler, N.; Jacquet, P.; Meigs, A.; Mailloux, J.; Menmuir, S.; Karhunen, J.; Lerche, E.; Monakhov, I.; Otin, R.; Thomas, B.; Dumortier, P.; Van Eester, D.; Barruzo, M.; Bobkov, V.; Brezinsek, S.; Colas, L.; Douai, D.; Milanese, D.; Pawelec, E.; Delabie, E.; Lomanowski, B.. - In: NUCLEAR FUSION. - ISSN 0029-5515. - ELETTRONICO. - 64:7(2024). [10.1088/1741-4326/ad5369]

Availability:

This version is available at: 11583/2989842 since: 2024-06-25T08:45:10Z

Publisher:

IOP Publishing Ltd

Published

DOI:10.1088/1741-4326/ad5369

Terms of use:

This article is made available under terms and conditions as specified in the corresponding bibliographic description in the repository

Publisher copyright

(Article begins on next page)

PAPER • OPEN ACCESS

ICRH-related impurity source and control across experiments in H, D, T plasmas at JET-ILW









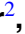
















To cite this article: A. Chomiczewska *et al* 2024 *Nucl. Fusion* **64** 076058

View the [article online](#) for updates and enhancements.

You may also like

- [Final report on the CCPR Key Comparison CCPR-K3.2014 Luminous Intensity](#)
Arnold A Gaertner, Éric Côté, Joaquin Campos et al.
- [APMP.QM-S19: Toxic elements in seafood](#)
Kelvin Chun-wai Tse, Wai-hong Fung, Mala Khan et al.
- [EURAMET.T-K.7 Comparison : Inter-laboratory comparison of triple point of water cells](#)
Murat Kalemci, Ali Uytun, Nedžadeta Hodži et al.

ICRH-related impurity source and control across experiments in H, D, T plasmas at JET-ILW

A. Chomiczewska^{1,*} , W. Gromelski¹ , I. Ivanova-Stanik¹ , E. Kowalska-Strzęciwilk¹ , N. Wendler¹ , P. Jacquet² , A. Meigs² , J. Mailloux² , S. Menmuir² , J. Karhunen¹¹ , E. Lerche^{2,3} , I. Monakhov² , R. Otin² , B. Thomas² , P. Dumortier³ , D. Van Eester³ , M. Barruzo⁴ , V. Bobkov⁵ , S. Brezinsek⁶ , L. Colas⁷ , D. Douai⁷ , D. Milanesio⁸ , E. Pawelec⁹ , E. Delabie¹⁰ , B. Lomanowski¹⁰  and JET Contributors^a

¹ Institute of Plasma Physics and Laser Microfusion, Warsaw, Poland

² UKAEA, Abingdon, United Kingdom of Great Britain and Northern Ireland

³ Laboratory for Plasma Physics, ERM/KMS, Brussels, Belgium

⁴ Dip.to Fusione e Tecnologie per la Sicurezza Nucleare, ENEA C. R. Frascati, Frascati, Italy

⁵ Max-Planck Institut für Plasmaphysik, Garching, Germany

⁶ Forschungszentrum Jülich, Institut für Energie- und Klimaforschung—Plasmaphysik, Jülich, Germany

⁷ CEA, IRFM, St-Paul-Lez-Durance, France

⁸ Politecnico di Torino, Torino, Italy

⁹ University of Opole, Opole, Poland

¹⁰ Oak Ridge National Laboratory, Oak Ridge, TN 37831, United States of America

¹¹ VTT Technical Research Centre of Finland, POBox 1000, Espoo, 02044 VTT, Finland

E-mail: agata.chomiczewska@ifpilm.pl

Received 15 January 2024, revised 17 May 2024

Accepted for publication 3 June 2024

Published 12 June 2024



Abstract

The experimental and theoretical analysis were focused on experiments conducted to assess the effect of plasma isotopes, protium (H), deuterium (D), and tritium (T) on ion cyclotron resonance heating (ICRH) related plasma wall interactions. Comparison of L-mode discharges with $N = 1$ ^3He and $N = 1$ H minority ICRH heating scenarios were done for different isotopes. For the selected pulses, the behaviour of high-Z, mid-Z and low-Z intrinsic impurity and radiated power behaviour was investigated based on data from VUV, visible spectroscopy, and bolometry diagnostic at Joint European Torus. It was found that for $N = 1$ ^3He scenario during radiofrequency antennas operation, core W, Ni content, Be source and the radiated power are higher for $\pi/2$ in comparison to dipole antenna phasing. Lowest core Ni, W content and radiated power is clearly observed for H plasmas in comparison to D and T, where for this ICRH scenario behaviour was similar. However, lower Be photon flux is observed for T in comparison to D plasmas. Be sputtering by He particles is responsible for such an effect. Additionally, several computer simulations were conducted using the COREDIV code. The difference in the electron temperature was due to the difference in the isotope masses. Increased temperature in the central plasma in the case of T plasmas leads to higher radiation in the central plasma in comparison to H plasmas. As a result, the power across separatrix is lower and the temperature

^a See Maggi *et al* 2024 (<https://doi.org/10.1088/1741-4326/ad3e16>) for JET Contributors.

* Author to whom any correspondence should be addressed.



Original content from this work may be used under the terms of the [Creative Commons Attribution 4.0 licence](https://creativecommons.org/licenses/by/4.0/). Any further distribution of this work must maintain attribution to the author(s) and the title of the work, journal citation and DOI.

on the divertor plate decreases with the increase of the isotope mass. At these temperatures on the divertor plate, W is not sputtered by the main plasma ions H, D and T and by He. For the $N = 1$ H ICRH scenario clear difference between D and T plasma was observed with higher metallic impurity content for T plasma in comparison to D. Impurity content in the plasmas is found to be sensitive to the power balance between the antenna straps. Its minimum is observed for the maximum of $P_{\text{cen}}/P_{\text{tot}}$.

Keywords: fusion, tokamak, impurities, ICRH, H isotopes

(Some figures may appear in colour only in the online journal)

1. Introduction

Ion cyclotron resonance heating (ICRH) is one of the main heating methods in the Joint European Torus (JET) tokamak, used to control impurities [1], for bulk heating of fuel ions [2, 3], and increase the energy of the plasmas. However, the interaction between the ICRH waves and the plasma can also lead to the transfer of energy and particles to the wall, i.e. plasma–wall interaction (PWI) [4, 5]. Plasmas are usually contaminated by intrinsic impurities. Elements with a high atomic number, like tungsten (W) can have a significant influence on fusion performance. This is of particular importance for tokamak devices with a metallic wall. One of the major challenges in achieving controlled fusion reactions is maintaining the right conditions for the fuel, usually isotopes of hydrogen, to undergo fusion and release energy. High Z impurities can affect this delicate balance. JET-ILW is well suited for extrapolation to ITER, due to its size, the full metal wall (W divertor and beryllium (Be) first wall [6]) and its unique capabilities to operate with tritium (T) and deuterium–tritium (D–T) fuel. At JET-ILW, the presence of W, Be and nickel (Ni), in the plasma is common [7, 8]. Controlling and minimizing the presence of high Z impurities is crucial. Extensive experimental work has been carried out to elucidate the origin of the isotope effect. Experimental campaigns in deuterium (D) (2019–2020), protium (H) (2020 with radiofrequency (RF)), T (2020–2021) and the second D–T experimental campaign (DTE2) (2021–2022) [9], addressed the impact of isotope effect on the PWI, core, scrape-off layer (SOL) and edge plasma physics to answer essential questions for magnetic fusion development that will affect ITER operation [10]. In particular, for the constant ELM frequency, the confinement showed a clear dependence on the isotope mixture. The pedestal density increase with effective mass was found to play a major role. The pedestal density isotope dependence was found to be similar to the pedestal pressure, pedestal particle confinement, and stored energy isotope dependence, while both the central electron and ion temperature show a reverse trend [11]. As it was reported in [12] for all isotopes the core confinement time increased with pedestal pressure due to electromagnetic turbulence stabilisation and profile stiffness. The changes in the pedestal density can also impact other aspects, for example, the plasma rotation which in turn affects the transport in the plasma core. In the ohmic plasmas, the global energy confinement was highest in T and lowest in H [13]. In D–T and

in T plasmas the transition from L-mode to H-mode requires less input power than in D, due to the reduction in the density value at which the power threshold is minimum [14]. In the dimensionless isotope mass scaling experiment, higher scaled energy confinement time is found in T in comparison to D plasmas [15]. In the Hybrid scenario, good access to H-mode with sustained high fusion power and controlled impurity radiation was obtained after re-optimisation of gas and power waveform. In the hybrid high performance plasmas, current ramp-up and q-profile were impacted by isotope mass [16] and the pulse with higher isotope mass had improved confinement [17]. However, the change in isotope from D to T led to a delay in the occurrence of type I ELMs after the H-mode entry resulting in very high edge radiation. The change of the isotopic mix from D to D–T in JET operations showed an increased incidence of neoclassical tearing modes (NTMs), in the Baseline scenario because of the higher β_N . NTM's are responsible for a decrease in plasma performances and leading in some cases to disruptions. In contrast, the Hybrid scenario with similar levels of β_N , resulting in a comparable magneto-hydrodynamic activity [18]. The sawtooth instabilities period tends to increase with high isotope mass [19]. For the same core plasma density, T plasmas were more strongly detached than H, D, D–T [20]. The impact of isotope mass on Be and W gross erosion was also investigated. The results showed the increase in Be physical sputtering yield and total W source from H to T [21, 22]. Higher power loads on the Be limiter, caused by Neutral Beam re-ionisation, and much cooler divertor target surfaces were observed in T plasmas than in their D [23]. Both phenomena are driven by SOL physics. The T plasmas had higher separatrix density and collisionality and broader SOL profiles which is beneficial for the power exhaust in the divertor. Isotopic effects were already observed in the first D–T campaign performed at the Tokamak Fusion Test Reactor in 1994 [24] and during the first D–T experimental campaign (DTE1) at JET executed in 1997 [25–28], however experiments at JET were performed in carbon wall (JET-C). Most PWI studies (and practically all on RF sheaths) in the literature were conducted in D plasmas, while fusion reactors will use other fuel mixtures. From the previous study, there is evidence that the RF-induced PWI is different between H and D plasmas but a strict comparison of H, D, and T plasmas for quantitative conclusions are missing. Therefore, the purpose of this paper is comparison of isotopes effect on ICRH related impurity sources and core plasma contamination. Analysis are

performed for two ICRH heating schemes, the fundamental helium-3 ($N = 1$ ^3He) and the fundamental hydrogen ($N = 1$ H) minority scenarios, respectively. In these scenarios, the ICRH waves have frequencies close to the frequency at which minority ions, gyrate around magnetic field lines. The notation $N = 1$ refers to the fundamental (first harmonic) of the ion cyclotron frequency that is being used to resonate with and heat the ions in the plasma. Previous experiments at JET with ^3He minority heating [29] and numerical prediction for ITER [10, 30] showed that plasmas with a ^3He concentration below 2% gave the best ion heating and fusion performance [10, 29]. Such heating scheme and 2nd harmonic of T are the reference ICRH scenario for ITER full-field ($B_T = 5.3$ T) D–T plasmas [10, 31]. The demonstration of ITER D–T ICRH scenarios was one of the objectives of the JET-DTE2 program. Dedicated experiments in DTE2 performed in T-rich plasmas with high D-NBI power highlighted the key impact of the fundamental D minority ICRH scenario which significantly increased the net fusion reactivity [2, 3]. Thereby, this ICRH scheme was a key ingredient to achieve a world record for the most fusion energy produced in a single fusion shot, by generating 59 MJ of heat from fusion reactions. That is more than twice the previous record of 22 MJ, also set at JET in 1997. The isotope effects are likely present in several aspects of the experiments (RF physics, transport, PWI) and need to be disentangled, if possible. A robust method is tested to mitigate this RF-related PWI. In section 2, the isotope impact on high-, mid- and low-Z impurity and plasma radiation for the fundamental ICR frequency of ^3He minority ICRH scenario is given. In section 3 the isotope effect on intrinsic impurities is analysed for the H minority ICRH scenario with power splitting between JET ICRH antenna straps. Both experimental and numerical modelling results are discussed. Finally, conclusions are given in section 4.

2. The fundamental ICR frequency of ^3He minority ICRH scenario in H, D and T

The experimental and theoretical analyses were focused on identical L-mode discharges performed in H, D and T plasmas at $B_T = 3.35$ T, $I_p = 2.15$ MA with both the inner and outer strike points on the horizontal W-coated divertor target plates (see figure 1(c)). Main species gas was adjusted to match, as far as possible, the SOL density in the pulses. The T stored in uranium beds was injected into the torus through dedicated tritium injection modules [32]. Helium (He) gas puff was used to apply the $N = 1$ ^3He minority ICRH scenario at resonance frequency $f = 32.5$ MHz. The ^3He concentration was $\sim 2\%$. The A2 ICRH antenna, comprising four antenna modules designated as A, B, C, and D, was employed in the experimental setup. A schematic top view depicting the spatial arrangement of modules A, B, C, and D is illustrated in figure 1(a). Antenna A + B and C + D were powered separately as an antenna pair via a 3 dB hybrid coupler network, and via an external conjugate-T network, respectively [33]. As it is presented in

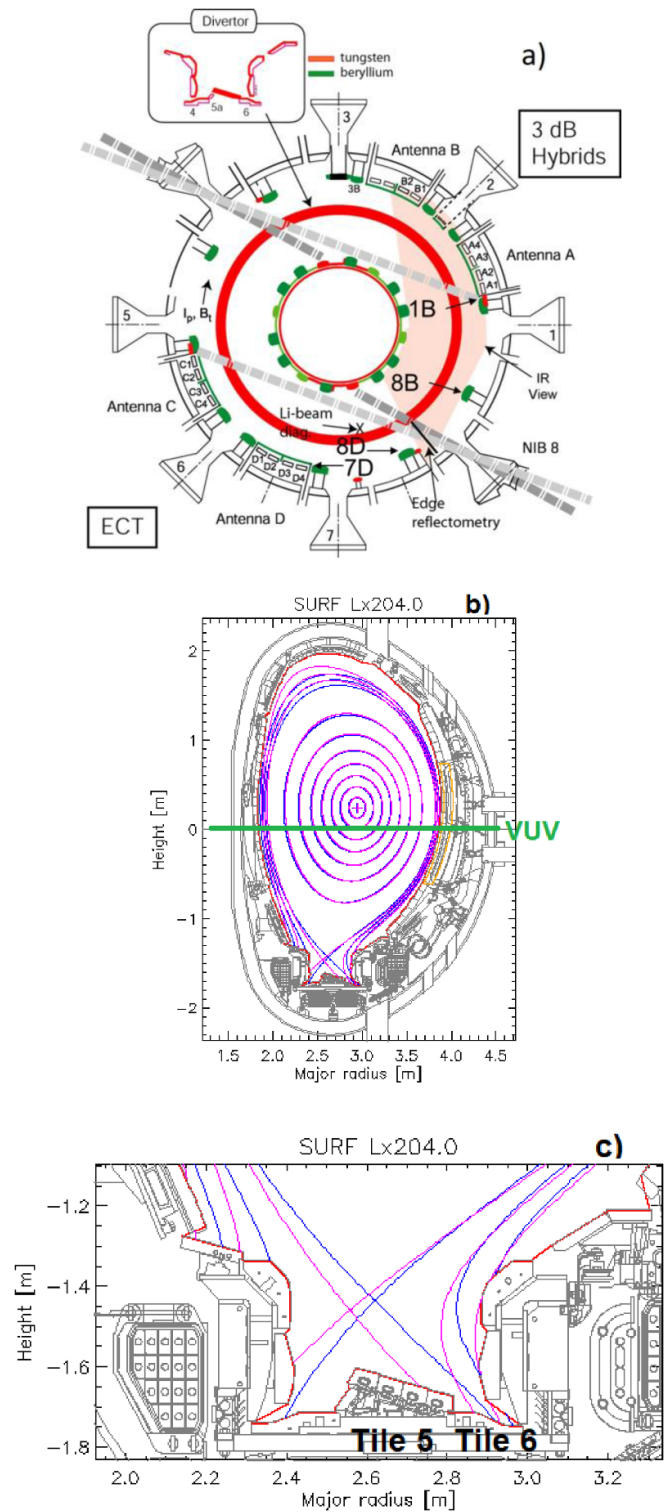


Figure 1. (a) Toroidal cross section of JET showing ICRH auxiliary heating system. Also showing Be (green) and W (red) plasma facing components. CXRS spectroscopy poloidal limiter locations 7D, 8D, 8B, 1B. (b) Poloidal cross section with the plasma configurations in $N = 1$ ^3He (blue) and $N = 1$ H (magenta) minority ICRH scenario with the lines of sight of JET VUV spectrometer (green horizontal line) and ICRH antenna (orange) at JET tokamak. (c) Magnetic configuration in the divertor with the outer strike point on tile 5 (in magenta) and tile 6 (in blue).

Table 1. List of analysed pulses with $N = 1$ ^3He ICRH scenario.

Antenna phasing	Hydrogen	Deuterium	Tritium
Dipole	#98371	#95644	#100127
$+\pi/2$	#98370	#95645	#100129

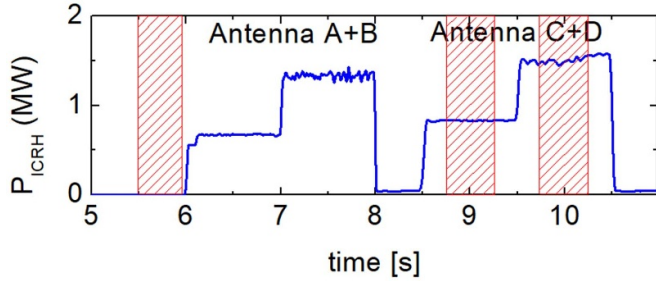
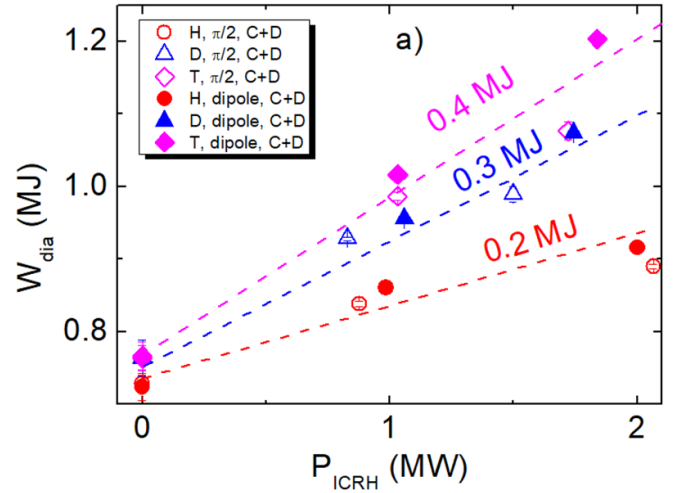
**Figure 2.** Time evolution of the launched ICRH power in #95645 by using two antennae in pair, with marked in red time intervals for calculations of average values plasma parameters.

figure 2, two power steps of ~ 1 MW and ~ 2 MW were applied using two RF antennae in pairs, either in dipole or $\pi/2$ antenna phasing, power balanced between straps. Changing the relative phasing between the four straps of the A2 antennas modifies the spectrum of the parallel wave number k_{\parallel} , resulting in different ICRH absorption by the plasma. The dipole antenna phasing is characterized by higher k_{\parallel} in comparison to $\pi/2$ antenna phasing [5]. The analysed discharges are listed in table 1. Since H shots suffered from bad antenna B phase control, which affects power coupling, heating efficiency and PWI, only the data in the ohmic phase and during C + D antenna pair operation were analysed. The experimental data has been averaged over the half-second period for each discharge in the ohmic phase and at 9 s and 10 s (see figure 2). Clear isotope effect on the heating performance and plasma confinement was observed. For the similar coupled ICRH power, the diamagnetic plasma energy (see figure 3) was 25% lower in D plasma and 50% lower in H plasma in comparison to T plasmas. An increase in the ICRH heating power from 0 to 2 MW resulted in an increase in diamagnetic energy by 0.2 MJ, 0.3 MJ and 0.4 MJ in H, D and T plasmas, respectively. The central electron temperature was highest for T plasmas and lowest for H plasmas. The same trend is observed and reported in the dedicated confinement experiments [11, 13].

2.1. Isotopic dependency of the plasma radiation, core high-, and mid-Z impurities

The behaviour of high-Z (W) and mid-Z (Ni) impurities and of the radiated power was investigated based on data from the JET VUV SPRED survey spectrometer [34], with the line-of-sight along the vessel mid-plane (see figure 1(b), green horizontal line) and the bolometry diagnostic [35]. As previously reported in [8], the source of Ni in JET tokamak is Inconel or Ni-based alloy components from which the JET vessel is constructed.

**Figure 3.** (a) Diamagnetic energy as a function of ICRH power in H, D, T plasmas for discharges with dipole or $\pi/2$ ICRH antenna phasing.

Ni is also associated with the operation of JET A2 ICRH antennas. As can be seen in figure 1(a), the main W source, marked in red, is the W divertor and in the main chamber NBI shine-through protection plates. Measurement of the Ni concentrations (c_{Ni}) in the plasmas were determined by the method described in detail in [36]. However, the quantitative measurement and comparison of W concentration was not possible due to disconnections of the SXR and XUV diagnostics, to protect them from damage when working with T. Such diagnostics were routinely used in previous studies [7, 8, 37, 38], before the first T injection. The VUV SPRED spectrometer records, within the wavelength range of 147–213 Å, the W feature characterized by multiple overlapping unresolved transition arrays of W-ions ranging from W^{14+} to W^{35+} . However, W measurement integrated in this wavelength range includes interfering lines due to other elements. Since these can be intense, an alternative measurement technique, denoted in this paper as I_{W} was proposed in [39] to mitigate such contamination. This alternative method involves computing the average of integrations centred on wavelengths of 176 Å and 201 Å, with a background subtraction of the integrated area about a wavelength of 142 Å. For each wavelength, an integration range technique was used, in which Simpson's rule was applied to the area defined by a certain number of pixels on either side of the wavelength centre. With 2048 pixels in the diagnostic detector, the integration range covered ± 5 pixels. This methodology was deemed the optimal compromise between minimizing blending and using a sufficient proportion of the line profile to ensure reliable measurements. In the ohmic phase of the analysed discharges, the rise of radiated power (see figure 4(a) for $P_{\text{ICRH}} = 0$) and Ni, W impurity content, due to the rise of isotope mass from H to T is observed, which suggests that isotope effects do exist without RF heating. Such effect is also observed during RF heating and can be seen in tomographic reconstructions of bolometry data, showing highest the radiated power density in T plasmas (figure 5). Observed higher plasma radiated

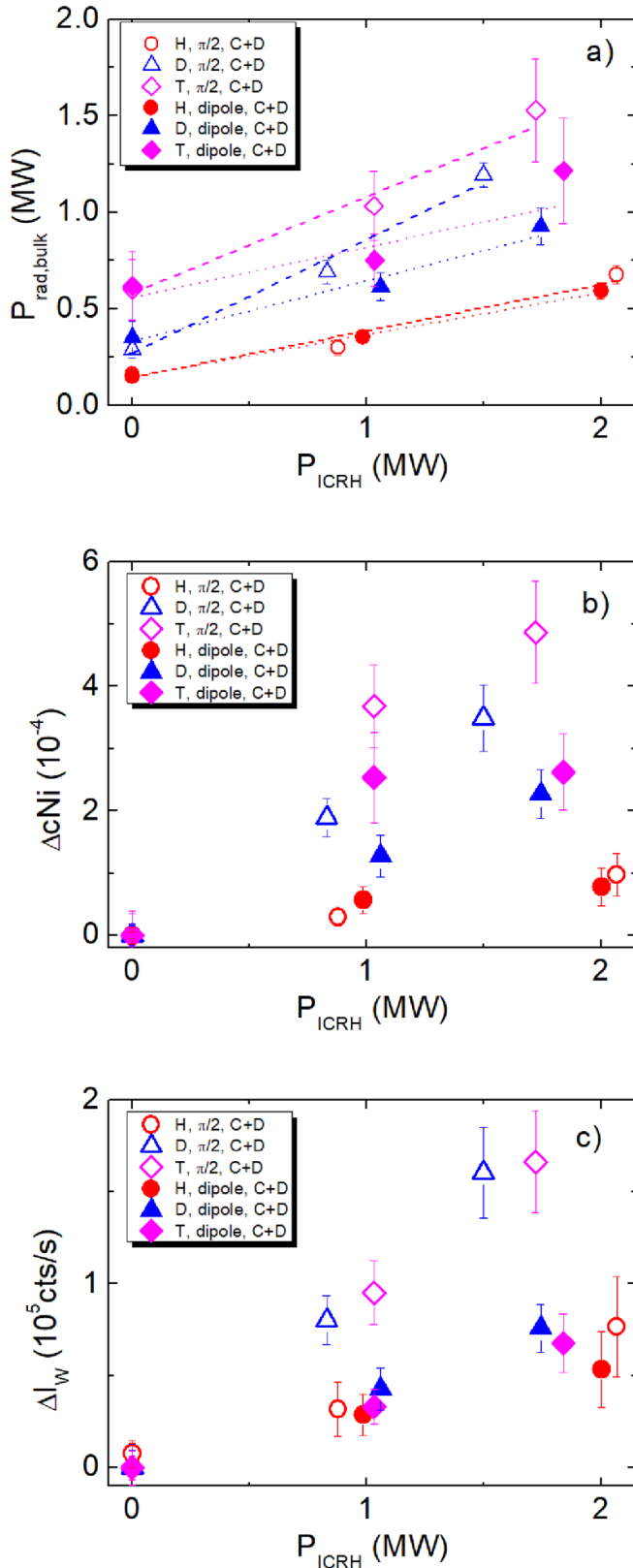


Figure 4. (a) The bulk radiated power, (b) ΔcNi and (c) ΔI_W (Data with subtracted impurity level in the ohmic phase) as a function of ICRH power for dipole or $\pi/2$ antenna phasing in H, D, T plasmas.

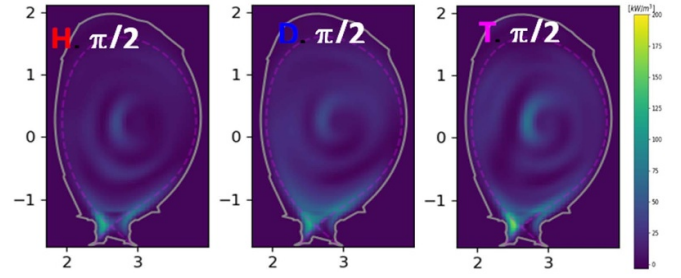


Figure 5. Tomographic reconstruction of the radiated power density at $t = 10$ s for the H pulse (left), D pulse (centre) and for the T pulse (right) in $\pi/2$ antenna phasing.

power proximal to the divertor is attributed to the emission of low-Z and mid-Z intrinsic impurities within the JET reactor. These impurities exhibit the highest cooling rate at lower temperatures. Conversely, fewer elements demonstrate significant radiative properties within the plasma core. The isotope effect on PWI is consistent with other JET experiments [22]. Therefore, to distinguish the RF-induced effects from isotopic effects, ΔcNi and ΔI_W are calculated for each discharge as a difference in the time-averaged value of the Ni concentration and W intensity during ICRH and that before the ICRH power is applied and presented in figures 4(b) and (c) for analysed pulses. Lowest values of ΔcNi and ΔI_W is found in H discharges, but no significant difference between D and T plasmas is observed. It was found that during ICRH Antenna operation the radiated power as well as Ni and W content in the central plasma is higher for $\pi/2$ antenna phasing compared to dipole antenna phasing (see figure 4). As it was also reported in [5], impurity content decreases with the parallel wave number $k_{||}$, which is higher in the case of dipole antenna phasing.

2.2. Isotopic dependency of Be source from the limiter

The change of impurity content in the plasma during ICRH can be attributed to an increase of impurity sources at the walls. JET is the only fusion device operating with Be limiters that protect the inner and outer first wall. This allowed studying Be sources in the main chamber and from ICRH antennas equipped with Be screen bars. The isotope effect, H versus D, on the Be effective sputtering yield, has been measured in Ohmic limiter plasmas in [21]. The Be erosion yield of D was about twice as high as that of H over the entire range of plasma densities studied. Also, the Z_{eff} of the D studied limiter plasmas was systematically larger compared to H ones. According to previous studies, the RF sheath rectification plays a significant role in the Be sputtering at the limiters near to or connected to active ICRF antenna along the magnetic field lines [40–42]. Charge exchange recombination spectroscopy (CXRS) is used on JET to study RF sheath-enhanced plasma–surface interactions in ICRF heated discharges [43]. The Be influx was diagnosed at four different outer poloidal limiter locations,

marked in figure 1(a) as 7D, 8D, 8B and 1B, which are close and far from the active antennas pair C + D. Observation spots are nearly centred on the limiter mid-plane. Figure 6 shows the effect of hydrogen isotopes on the local BeII spectral line emission at 467 nm for the observation location 7D and 1B marked in figure 1(a). Changing H by D, the RF-induced Be source was increasing with the isotope mass. Higher Be photon flux is observed for $\pi/2$ antenna phasing in comparison to dipole phasing in D, T and H plasmas. This trend is observed for all analysed lines of sight. As it is presented in [44], Be sputtering yield by He particles is stronger than by D and T. This effect explains the observed greater BeII intensity for D in comparison to T plasmas for which the measured ^3He minority concentration during the ICRH phase was $^3\text{He}[\text{X}] \sim 2\%$ and $^3\text{He}[\text{X}] \sim 0.8\%$, respectively. The experimental value of $^3\text{He}[\text{X}]$ was calculated based on the *Optical Penning Gauge* technique, used for the measurement of the fuel isotopic composition and He concentration from a high-resolution spectrometer [45]. It can be seen in figure 6(a) that the difference between D and T points is notably greater than that observed in figure 6(b). This divergence can be attributed to the heightened influence of ^3He on Be production at position 7D, which resides in closer proximity to the active antennas C and D, as opposed to position 1B, situated at a greater distance from the active antennas. This observation implies that the local RF electric field may contribute significantly to the acceleration of ^3He particles towards the reactor wall. To highlight the larger Be sputtering in T plasmas in comparison to D and H, the BeII brightness presented in figures 6(a) and (b) was normalized to $^3\text{He}[\text{X}]$ (see figures 6(c) and (d)). Additional analysis performed on another data set showed that for higher $^3\text{He}[\text{X}]$, higher BeII intensity is observed at different limiter locations. However, the ^3He concentration was not found to affect the Ni and W content in the plasmas.

Be sputtering can be sensitive to the electrical settings of the antenna if the sheath potentials explore a domain where sputtering yields Y_{eff} varies with the accelerating voltages driven by ICRF fields. To highlight some expected differences between H/D/T and to illustrate the effect of sheath rectification on the W and the Be sputtering, theoretical curves of gross erosion Y_{eff} versus accelerating voltage were calculated based on formulas presented in [46].

As can be seen in figure 7, W sputtering increases with the isotope mass of the majority species, but no isotope effect on W production is expected if the sheath voltage does not exceed 150 V in T, 250 V in D and 500 V in H. At lower sheath voltage, the sputtering is likely dominated by light impurities. This is illustrated by adding to the plot 2% of $^3\text{He}^{2+}$ ions on the plasma mix. Unlike W, lower values of accelerating voltages are needed for Be sputtering. The Y_{eff} for the Be, presented in figure 8, is rather flat for accelerating voltages >50 V. Thus, Be should be influenced by the sheath rectification effect. Also, the isotope effect of the majority species is expected. However, in D and T plasmas weak effect of the light impurities is expected for voltages >50 V.

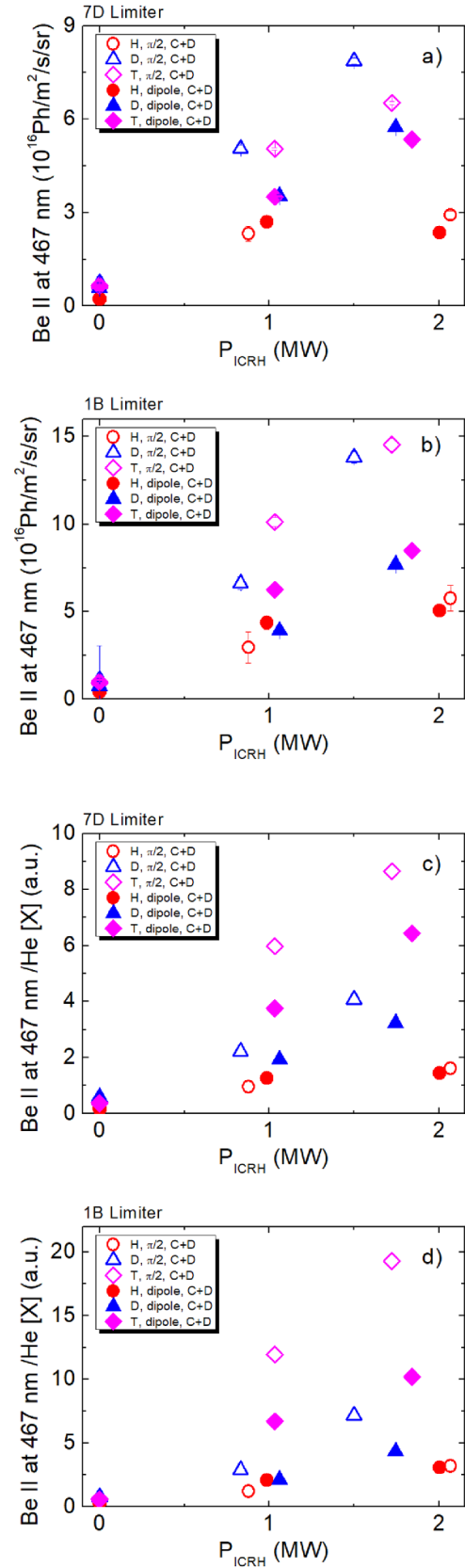


Figure 6. BeII at 467 nm line emission, measured at outer poloidal limiter locations (a) 7D and (b) 1B, BeII/He[X] measured at locations (c) 7D and (d) 1B as a function of ICRH power for dipole or $\pi/2$ antenna phasing in H, D, T plasmas.

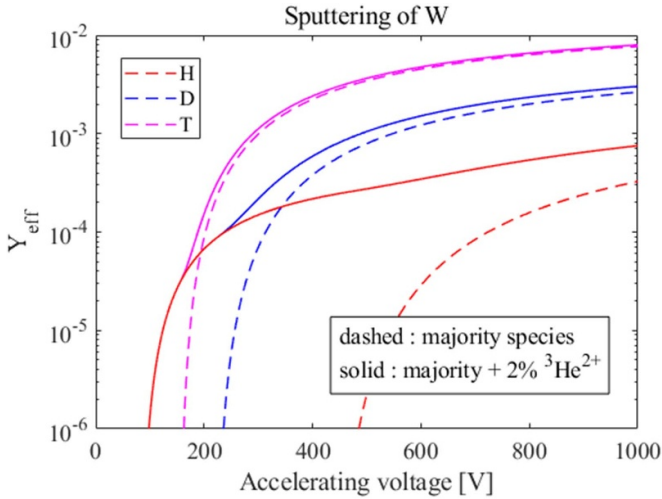


Figure 7. Theoretical curves for W gross erosion by H, D and T isotopes (dashed lined) and the mix of majority plasma ions with 2% $^3\text{He}^{2+}$ as a function of accelerating voltage.

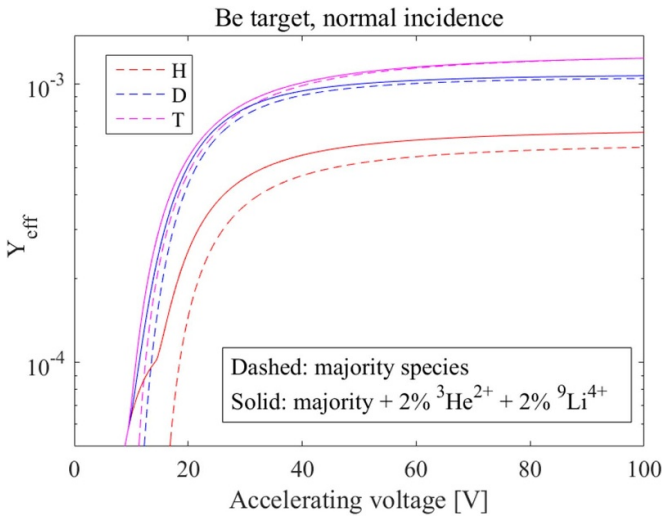


Figure 8. Theoretical curves for Be gross erosion sputtering yields by H, D and T isotopes (dashed lined) and the mix of majority plasma ions with 2% $^3\text{He}^{2+}$ + 2% $^9\text{Li}^{4+}$ as a function of accelerating voltage.

2.3. Modelling with the COREDIV code

the COREDIV code [47–49], which couples self-consistently the plasma core with the SOL, and the impurities with the main plasma. In this study, four impurities are considered, Be, Ni, W and He. The Be, Ni, and He fluxes are given as code inputs while the W flux is self-consistently computed as dependent on the fluxes of Be, Ni, He and on self-sputtering. The main inputs of the code are the plasma volume averaged electron density, the input power, the plasma thermal energy, and the main ion and impurity transport coefficients. The discharges with $\pi/2$ antenna phasing, listed in table 1, were simulated. Two time points at $t = 9$ s and $t = 10$ s, characterized by different heating powers were selected for the analysis. Given the consistency in conclusions, the subsequent discussion is founded upon the

outcomes derived from the second time point. The numerical results for $t = 10$ s are compared with the experimental profiles of electron temperature and density from high resolution Thomson scattering diagnostic (see figure 9), source temperature at the LFS strike point on the divertor plate (T_e^{PLATE}), W, Ni, Be, He impurity concentrations, effective charge state (Z_{EFF}), total radiated power (R^{TOTAL}), core radiated power (R^{CORE}) and SOL radiated power (R^{SOL}). A comparison of the main plasma parameters is provided in table 2. A good agreement between experimental and simulated kinetic profiles was achieved (see figure 9). Similar n_e profiles were obtained in H, D and T plasmas. The observed difference in T_e was due to the difference in the isotope mass. Increased T_e in the central plasma in the case of T leads to higher plasma radiation in the central plasma in comparison to H and D plasmas. As a result, the power across the separatrix is lower and T_e^{PLATE} decreases with the increase of the isotope mass. The simulations are consistent with the measurements that show the reduction of the electron temperature at the LFS strike point. T_e^{PLATE} measured by the Langmuir probe was 7.19 eV, 5.9 eV and 3.9 eV for H, D and T plasmas, respectively. It must be noted that the probes measurements in such temperature range are moderately accurate. Accordingly, the largest temperature measured by the protection camera looked at the horizontal W-coated outer target plate (see figure 1(c), Tile 6), was 820 °C, 700 °C and 550 °C.

In these electron temperature conditions on the divertor plates, W is not sputtered by the main plasma ions H, D and T nor by the He minority. It turned out that in the examined plasmas W is sputtered mainly by Be and Ni. Simulations showed that the Ni radiation in the central plasma is 0.34 MW for H, 0.62 MW for D and 0.77 MW for T plasma and this is about 50% of the core radiated power. At lower heating power in T plasmas, Be does not affect W production. Additional simulations for T plasmas with the change of Be content were addressed to assess its influence on plasma parameters. For this purpose, simulations with two different Be streams $C_{\text{Be}} = 0.7\%$ and $C_{\text{Be}} = 2.17\%$, were performed. It was observed that the Be affects the Z_{EFF} , increasing its value from 1.3 to 1.48. However, for the prevailing temperatures on the divertor plate, it does not affect W production. The higher value of Be content had a very weak effect on plasma radiation.

3. Power splitting between straps in H minority ICRH scenario in D and T plasmas

The influence of ICRH on the PWI was also studied running identical D (#94998) and T plasmas (#100187) with $B_T = 3$ T, $I_p = 1.8$ MA, in low triangularity L-mode plasma with the inner and outer strike-line on the vertical W-coated and on the semi-horizontal bulk-W target plates (tile 5, see figure 1(c)). The fundamental hydrogen minority $N = 1$ H ICRH scenario at resonance frequency $f = 42.5$ MHz was utilized for the experiment. Discharges were run with A2 antenna D only and dipole antenna phasing. As it can be seen in figure 10(a), in D plasmas 1 MW of ICRH power was launched, however in the T case only 0.5 MW. Higher power would saturate Be-line

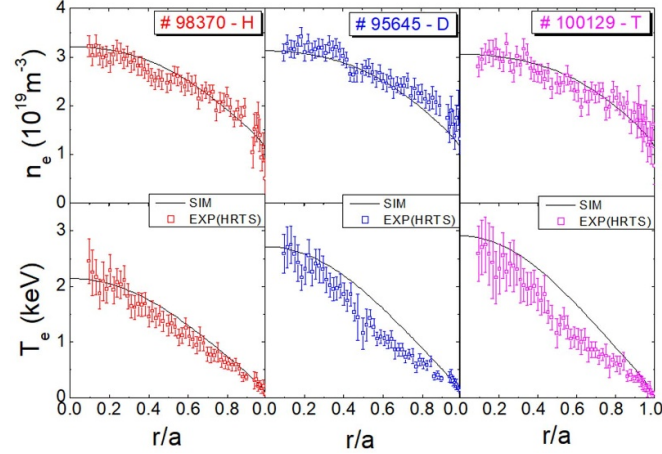


Figure 9. Experimental electron density (n_e) and temperature (T_e) profiles, for pulses #98370, #95645 and #100129 at the considered time $t = 10$ s and the corresponding COREDIV computed profiles.

Table 2. Main plasma parameters with experiment and simulations for $t = 10$ s.

Parameter	#98370(H)		#95645(D)		# 100129(T)	
	EXP	SIM	EXP	SIM	EXP	SIM
P_{OH} (MW)	1.2	1.2	1.2	1.2	1.2	1.2
P_{aux} (MW)	1.5	1.5	1.5	1.5	1.8	1.8
T_e^{PLATE} (eV)	7.19	17.1	5.9	14.3	3.9	11.6
C_W ($\times 10^{-5}$)	—	2.79	—	2.04	—	1.57
C_{Ni} ($\times 10^{-5}$)	11.6	11.5	39	39.5	49	48.6
C_{Be} (%)	—	1.52	—	1.94	—	1.59
C_{He} (%)	2	1.9	2	2.0	0.8	0.8
Z_{EFF}	1.4	1.4	1.66	1.63	—	1.74
R^{TOTAL} (MW)	1.17	1.18	1.67	1.75	2.0	1.86
R^{CORE} (MW)	0.7	0.66	1.06	1.23	1.5	1.18
R^{SOL} (MW)	0.47	0.52	0.61	0.53	0.5	0.67

spectroscopy in the T plasmas. However, in such conditions similar density and temperature profiles were obtained, therefore the comparison of discharges in a quantitative way was possible. Then our data were normalized to ICRH power to get rid of the power effect. In all discharges, a scan of the power partition between the inner/outer straps of one of A2 antenna D was performed aiming at minimising the RF-sheath rectification effect.

The fraction of power from the inner straps to total power P_{cen}/P_{tot} is illustrated in figure 10(a). Enhanced RF-PWI are observed in T plasmas. Bulk radiated presented in figure 10(b) power is higher in T plasmas in comparison to D plasmas. The production of neutral Be atoms depends on the isotope, T plasmas showing higher Be neutral particle fluxes than D plasmas (see figure 10(c)). Indeed, the BeI line intensity is found to be sensitive to the power balance between the antenna straps for a given dipole antenna phasing, as the metallic Ni (see figure 10(d)) and W (see figure 10(e)) impurity content in the plasma is affected. The minimum in the radiated power and impurity content is observed for the maximum of P_{cen}/P_{tot} . The optimal RF setting is isotope independent. Reduction of the RF-driven PWI for $P_{cen}/P_{tot} \sim 0.8$ is consistent with the A2 antenna near field calculation and

the ICRH antenna optimisation concept presented in [50]. Different hypotheses are under consideration, to explain the difference between D and T plasmas in this experiment. For example, an increased Be sputtering yield by T, or invoking slow wave properties in the SOL and larger RF-sheath rectification with T. At JET-ILW, W impurities come mainly from W divertor baffles, however, it must be noted that they can also be sputtered from PFCs located in the main chamber, such as the NBI shine-through protection plates. Also, high-Z impurities migrate throughout the vessel and can be deposited in the main chamber limiters. In the present study, the effect of RF power balance on impurity behaviour is mostly observed in the limiter region and not observed in the divertor W source. This can be seen in figure 8(f) showing neutral WI emission at 400.9 nm from the outer divertor derived from the combination of the signals detected by the divertor spectroscopy and the W filterscope diagnostics to separate the contribution of the plasma continuum. This is an identical approach to the one described in [51, 52]. Additionally, the WI signal is normalized to ion flux to the divertor plate. The divertor W source is lower for T plasmas in comparison to D. This is explained by the lower power across the separatrix and lower divertor plate temperature with the increased

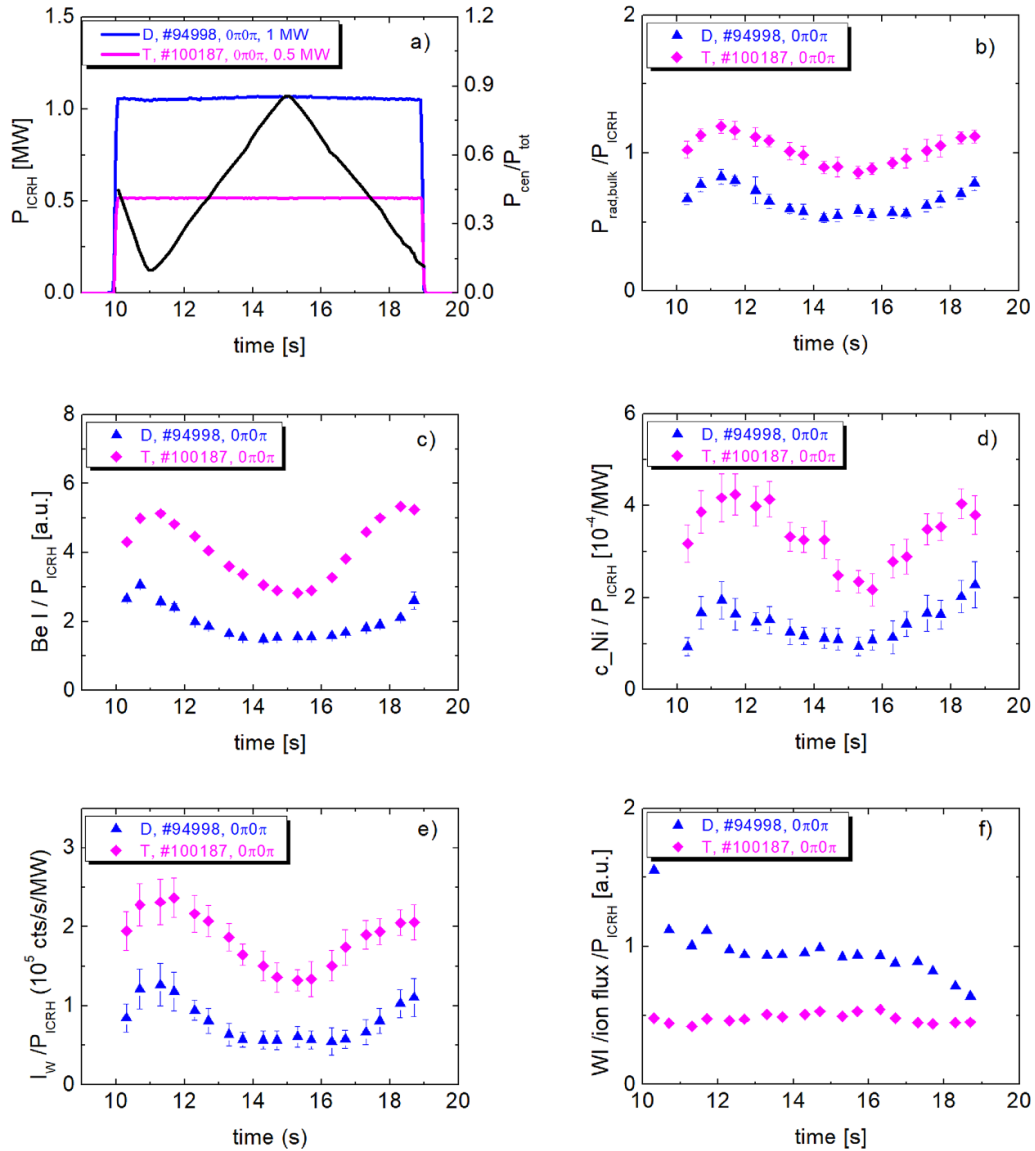


Figure 10. Comparison of (a) launched ICRH power and fraction of power from the inner straps, (b) bulk radiated power, BeI at 457 nm line emission measured at outer poloidal limiters locations 7D, (d) Ni concentration and (e) W quasicontinuum intensity and (f) WI line emission at 400.9 nm from the divertor (normalised to 1 MW of ICRH power), for the time evolution of D pulse (#94998) and T pulse (#100187).

isotope mass obtained from COREDIV simulations and the experimental data. The electron temperature near the divertor target was measured by both, Langmuir probes and the line-integrated plasma emission spectroscopy using the Balmer photo-recombination continuum feature [53]. For the conditions achieved in the experiment, the temperature along the divertor plate with the separatrix is in the range of 2–8 eV in T plasmas, in which case W is not sputtered by hydrogen isotopes [54]. This suggests that W sputtering in the divertor region is mainly due to Be and Ni impurities. A reliable probe or spectroscopic measurement for D plasmas was not possible. However, the protection camera looked at the semi-horizontal bulk-W target plates (see figure 1(c), Tile 5), measured maximum temperature of 660 °C for D plasmas and 520 °C for T plasmas. Indicating a higher load with 1 MW in D than with 0.5 MW in T.

4. Conclusions

The increase of plasmas radiated power with isotope mass was measured and the increase of W, Ni impurity content in the plasmas is confirmed. Such behaviour is related to the increase in Be physical sputtering yield from H to T. In addition to normal plasma effects, there are those associated with ICRH. Results from recent experiments demonstrate that the ICRH-specific impurity release can differ significantly depending on the ICRH scenario and minority content as well as hydrogen isotopes constituting the plasma, with T-plasmas showing higher impurity content compared to D and H plasmas. Application of the $N = 1$ 3He minority ICRH scenario in ITER will require measurements and control of helium concentration because as it was found for JET-ILW it can play a major role in Be sputtering. The effect of ICRH on impurity

behaviour is mostly observed in the limiter region, highlighting the important role of the RF-sheath rectification effect and induced potential driven by the existence near the antenna of an RF electrical field component E_{\parallel} , parallel to the magnetic field. This potential leads to the acceleration of plasma particles towards the first wall which causes impurity sputtering. Due to the lower power across the separatrix and lower divertor plate temperature, obtained from COREDIV simulations and the experimental data, the W source from the divertor is lower with the increased isotope mass in this experiment. JET A2 Antenna RF modelling using the TOPICA [55] and ERMES [56] code is ongoing in support of this experiment. Both codes predict a slightly higher electric field in front of the antenna in T plasmas as compared to D. Some more work is required to understand code results in H plasmas. Also, in ERMES strong toroidal asymmetries in the field pattern in front of the antenna are observed in the case of D and T which still need to be understood/explained. A detailed report will be the subject of future publications. ICRH-specific PWI such as those observed at JET tokamak must be considered in the development of heating scenarios in ITER. RF settings were found on A2 antennas that can reduce the RF-related impurity production near the antenna for 2 isotopes at least. Simulations in [52] suggest that similar settings exist on the ITER antenna. These do not reduce excessively the maximum coupled power.

Acknowledgments

This scientific paper has been published as part of the international project co-financed by the Polish Ministry of Science and Higher Education within the programme called ‘PMW’ for 2024. This work has been carried out within the framework of the EUROfusion Consortium, funded by the European Union via the Euratom Research and Training Programme (Grant Agreement No. 101052200—EUROfusion). Views and opinions expressed are however those of the author(s) only and do not necessarily reflect those of the European Union or the European Commission. Neither the European Union nor the European Commission can be held responsible for them.

ORCID iDs

A. Chomiczewska <https://orcid.org/0000-0003-4931-728X>
 W. Gromelski <https://orcid.org/0000-0003-2683-8453>
 I. Ivanova-Stanik <https://orcid.org/0000-0002-2766-8612>
 E. Kowalska-Strzeczniak <https://orcid.org/0000-0003-1710-9806>
 N. Wendler <https://orcid.org/0000-0002-9765-6027>
 P. Jacquet <https://orcid.org/0009-0007-9916-2032>
 A. Meigs <https://orcid.org/0000-0002-8071-864X>
 J. Mailloux <https://orcid.org/0009-0005-4265-5480>
 J. Karhunen <https://orcid.org/0000-0001-5443-518X>
 E. Lerche <https://orcid.org/0000-0003-4584-3581>
 I. Monakhov <https://orcid.org/0009-0009-2936-5605>
 R. Otin <https://orcid.org/0000-0002-3053-2695>
 P. Dumortier <https://orcid.org/0000-0002-6372-5450>

D. Van Eester <https://orcid.org/0000-0002-4284-3992>
 M. Barruzo <https://orcid.org/0009-0006-7853-7280>
 V. Bobkov <https://orcid.org/0000-0002-2328-9308>
 S. Brezinsek <https://orcid.org/0000-0002-7213-3326>
 L. Colas <https://orcid.org/0000-0002-4573-3326>
 D. Douai <https://orcid.org/0009-0002-6980-9927>
 D. Milanese <https://orcid.org/0000-0002-5114-7235>
 E. Pawelec <https://orcid.org/0000-0003-1333-6331>
 E. Delabie <https://orcid.org/0000-0001-9834-874X>
 B. Lomanowski <https://orcid.org/0000-0003-2226-2004>

References

- [1] Lerche E. et al 2016 *Nucl. Fusion* **56** 036022
- [2] Maslov M. et al 2023 *Nucl. Fusion* **63** 112002
- [3] Lerche E. et al 2023 Fundamental ICRF heating of deuterium ions in JET-DTE 2023 29th IAEA Fusion Energy Conf. (London, United Kingdom, 16–21 October 2023)
- [4] Bobkov V. et al 2017 *Nucl. Mater. Energy* **12** 1194
- [5] Czarnecka A. et al 2012 *Plasma Phys. Control. Fusion* **54** 074013
- [6] Matthews G.F. et al 2013 *J. Nucl. Mater.* **438** S2–S10
- [7] Sertoli M., Carvalho P.J., Giroud C. and Menmuir S. 2019 *J. Plasma Phys.* **85** 905850504
- [8] Czarnecka A. et al 2019 *Plasma Phys. Control. Fusion* **61** 085004
- [9] Maggi C.F. et al 2024 Overview of T and D-T results in JET with ITER-like Wall 2024 29th IAEA Fusion Energy Conf. 2023 (London, United Kingdom, 16–21 October 2023)
- [10] Mailoux J. et al 2022 *Nucl. Fusion* **62** 042026
- [11] Frasinetti L. et al 2023 *Nucl. Fusion* **63** 112009
- [12] Shneider P.A. et al 2023 *Nucl. Fusion* **63** 112010
- [13] Delabie E. et al 2023 The isotope effect on core heat transport in JET-ILW ohmic plasmas in hydrogen, deuterium and tritium 2023 29th IAEA Fusion Energy Conf. (London, United Kingdom, 16–21 October 2023)
- [14] Solano E. et al 2023 *Nucl. Fusion* **63** 112011
- [15] Tala T. et al 2023 *Nucl. Fusion* **63** 112012
- [16] Challis C.D., Brezinsek S., Coffey I.H., Fontana M., Hawkes N.C., Keeling D.L., King D.B., Pucella G. and Viezzer E. 2020 *Nucl. Fusion* **60** 086008
- [17] Hobirk J. et al 2023 *Nucl. Fusion* **63** 112001
- [18] Alessi E. et al 2023 Comparison of MHD onset conditions in JET-ILW experiments 2023 29th IAEA Fusion Energy Conf. (London, United Kingdom, 16–21 October 2023)
- [19] Nowak S. et al 2023 Sawteeth dynamics in JET Baseline discharges with mixtures of isotopes 2023 29th IAEA Fusion Energy Conf. (London, United Kingdom, 16–21 October 2023)
- [20] Groth M. et al Impact of H, D, T and D-T hydrogenic isotopes on detachment in JET ITER-like Wall low-confinement mode plasmas Preprint: 2023 29th IAEA Fusion Energy Conf. (London, United Kingdom, 16–21 October 2023)
- [21] De La Cal E. et al 2022 *Nucl. Fusion* **62** 126021
- [22] Douai D. et al 2023 Overview of plasma-wall interactions studies in JET-ILW H, D, T and DT campaigns 2023 29th IAEA Fusion Energy Conf. (London, United Kingdom, 16–21 October 2023)
- [23] Sun H.J. et al 2023 *Nucl. Fusion* **63** 016021
- [24] Scott S.D. et al 1995 *Phys. Plasmas* **2** 2299–307
- [25] Keilhacker M. et al 1999 *Nucl. Fusion* **39** 209
- [26] The JET Team 1999 *Nucl. Fusion* **39** 1227
- [27] Bhatnagar V.P. et al 1999 *Nucl. Fusion* **39** 353
- [28] JET Team 1999 *Nucl. Fusion* **39** 1763
- [29] Mantsinen M. et al 2023 *Nucl. Fusion* **63** 112015
- [30] Bilato R. et al 2014 *AIP Conf. Proc.* **1580** 291

- [31] Jacquet P. et al 2023 *AIP Conf. Proc.* **2984** 030003
- [32] Belonohy E. et al 2017 *Fusion Eng. Des.* **123** 196–200
- [33] Graham M. et al 2012 *Plasma Phys. Control. Fusion* **54** 074011
- [34] Fonck R.J., Ramsey A.T. and Yelle R.V. 1982 *Appl. Opt.* **21** 2115
- [35] Huber A. et al 2007 *Fusion Eng. Des.* **82** 1327
- [36] Czarnecka A., Zastrow K.-D., Rzadkiewicz J., Coffey I.H., Lawson K.D. and O'Mullane M.G. 2011 *Plasma Phys. Control. Fusion* **53** 035009
- [37] Pütterich T. et al 2013 *Plasma Phys. Control. Fusion* **55** 124036
- [38] Krawczyk N., Czarnecka A., Ivanova-Stanik I., Zagórski R., Challis C., Frigione D., Giroud C., Graves J., Mantsinen M.J. and Silburn S. 2018 *Rev. Sci. Instrum.* **89** 10D131
- [39] Lawson K.D., Coffey I.H., Rimini F. and Książek I. 2021 *Plasma Phys. Control. Fusion* **63** 105001
- [40] Klepper C.C. et al 2013 *J. Nucl. Mater.* **438** S594–8
- [41] Jacquet P. et al 2014 *Phys. Plasmas* **21** 061510
- [42] Klepper C.C. et al 2016 *Phys. Scr.* **2016** 014035
- [43] Klepper C. et al 2017 *EPJ Web Conf.* **157** 03024
- [44] Brezinsek S. et al 2022 *25th Int. Conf. on Plasma Surface Interaction in Controlled Fusion Devices (PSI-25)* (12 January 2022)
- [45] Vartanian S. et al 2021 *Fusion Eng. Des.* **170** 112511
- [46] Behrisch R. and Eckstein W. (Rainer Behrisch, Wolfgang Eckstein) 2007 *Sputtering by Particle Bombardment: Experiments and Computer Calculations from Threshold to MeV Energies* (Springer) Topics in Applied Physics vol. 110 Stankiewicz R et al 2001 *J. Nucl. Mater.* **290–293** 738–42
- [47] Zagorski R., Ivanova-Stanik R.I. and Stankiewicz R. 2013 *Nucl. Fusion* **53** 073030
- [48] Stankiewicz R. and Zagórski R. 2003 *J. Nucl. Mater.* **313–6** 899–903
- [49] Telesca G. et al 2021 *Nucl. Fusion* **61** 066027
- [50] Bobkov V. et al 2019 *Nucl. Mater. Energy* **18** 131
- [51] Den Harder N., Brezinsek S., Pütterich T., Fedorczak N., Matthews G.F., Meigs A., Stamp M.F., van de Sanden M.C.M. and Van Rooij G.J. 2016 *Nucl. Fusion* **56** 026014
- [52] Huber A. et al 2020 *Nucl. Mater. Energy* **25** 100859
- [53] Lomanowski B., Groth M., Coffey I., Karhunen J., Maggi C.F., Meigs A.G., Menmuir S. and O'Mullane M. 2020 *Plasma Phys. Control. Fusion* **62** 065006
- [54] Brezinsek S. et al 2019 *Nucl. Fusion* **59** 096035
- [55] Milanesio D., Meneghini O., Lancellotti V., Maggiora R. and Vecchi G. 2009 *Nucl. Fusion* **49** 115019
- [56] Otin R. 2020 *AIP Proc.* **2254** 050009